Journal of Climate

Enhanced Efficacy Amplifies Tropical Cyclones Intensification in Warmer Climates

--Manuscript Draft--

Manuscript Number:	JCLI-D-25-0570
Full Title:	Enhanced Efficacy Amplifies Tropical Cyclones Intensification in Warmer Climates
Article Type:	Article
Corresponding Author:	Bosong Zhang UNITED STATES
Corresponding Author's Institution:	
First Author:	Bosong Zhang
Order of Authors:	Bosong Zhang
	Brian Soden
	Gabriel Vecchi
	Wenchang Yang
Abstract:	Tropical cyclones (TCs) are expected to intensify in a warming climate as sea surface temperatures (SSTs) rise. Potential intensity (PI), the thermodynamic upper limit on storm strength, has long been used to assess how environmental conditions constrain TC intensity. However, a storm's realized strength also depends on the efficacy in approaching its PI. Using a high-resolution (25 km) global TC-permitting model, we show that uniform SST warming strengthens TCs through concurrent increases in PI and efficacy, leading to a marked rise in the frequency of Category 3–5 storms. The increased efficacy persists even when changes in wind shear and ventilation effects are accounted for, indicating that changes in TC ventilation is not a primary driver for the increased efficacy. This dual increase in thermodynamic limits and storm efficacy underscores the importance of considering both PI and efficacy when projecting future TC risks, as considering only increased PI may underestimate intensification in a warmer climate. The development of a theory for the environmental controls on efficacy is needed to close our theoretical expectation and extract the greatest predictability for the response of TC intensity to climate change and variations.
Suggested Reviewers:	

Enhanced Efficacy Amplifies Tropical Cyclones Intensification in Warmer Climates

Bosong Zhang[1], Brian J. Soden[2], Gabriel Vecchi[3,4], Wenchang Yang[3]

1. Program in Atmospheric and Oceanic Sciences, Princeton University, Princeton, NJ, USA
2. Rosenstiel School of Marine, Atmospheric and Earth Science, University of Miami, Miami, FL, USA
3. Department of Geosciences, Princeton University, Princeton, NJ, USA
4. High Meadows Environmental Institute, Princeton University, Princeton, NJ, USA

Corresponding author: Bosong Zhang (bosongzhang@gmail.com)

Abstract

Tropical cyclones (TCs) are expected to intensify in a warming climate as sea surface temperatures (SSTs) rise. Potential intensity (PI), the thermodynamic upper limit on storm strength, has long been used to assess how environmental conditions constrain TC intensity. However, a storm's realized strength also depends on the efficacy in approaching its PI. Using a high-resolution (25 km) global TC-permitting model, we show that uniform SST warming strengthens TCs through concurrent increases in PI and efficacy, leading to a marked rise in the frequency of Category 3–5 storms. The increased efficacy persists even when changes in wind shear and ventilation effects are accounted for, indicating that changes in TC ventilation is not a primary driver for the increased efficacy. This dual increase in thermodynamic limits and storm efficacy underscores the importance of considering both PI and efficacy when projecting future TC risks, as considering only increased PI may underestimate intensification in a warmer climate. The development of a theory for the environmental controls on efficacy is needed to close our theoretical expectation and extract the greatest predictability for the response of TC intensity to climate change and variations.

Significance Statement

Tropical cyclones (including hurricanes and typhoons) are expected to get stronger as the oceans warm (e.g. (Knutson et al. 2020)). A prediction for this expected increase in TC intensity was based on the theory of potential intensity (PI) (Emanuel 1999). PI can serve as a basis to estimate and interpret TC intensity change under given environmental conditions. But a storm's actual strength also depends on how efficiently it can use this available energy, which is referred to as relative intensity (**r**), or efficacy–the ratio of actual intensity to PI. Using a high-resolution climate model, we find that warming oceans not only raise the ceiling for storm strength (higher PI) but also make storms more efficient at reaching this limit (higher r). Importantly, this increase in efficacy is not explained by changes in wind shear or ventilation, but by the fact that warmer oceans provide favorable conditions for longer periods of time. Together, in this model, these effects lead to stronger and more frequent major hurricanes (Category 3–5). This means that climate projections based only on PI may underestimate the risks posed by tropical cyclones in a warming world.

1. Introduction

Tropical cyclones (TCs) are powerful convective systems characterized by concentrated water vapor and deep cloudiness, producing severe impacts through intense winds, heavy rainfall, and storm surges. Understanding the physical mechanisms that govern TC development—and how these storms respond to rising greenhouse gas concentrations and warming sea surface temperatures (SSTs)—is essential for improving climate projections and mitigating TC-related risks.

Projections of future TC activity remain uncertain (Camargo et al. 2023; Knutson et al. 2020), partly due to limitations in the spatial resolution of global climate models (Roberts et al. 2020). Environmental indicators from coarse-resolution models have suggested a potential decline in global TC frequency under a high-emission scenario (Camargo et al. 2025). In contrast, several studies suggest an increase in the occurrence of rapid intensification events across multiple ocean basins (Bhatia et al. 2022; Song et al. 2020). Results from downscaled model projections indicate an increase in both TC frequency and severity (Emanuel 2021). Observational data also indicate a trend toward more intense TCs, likely linked to rising SSTs that foster favorable conditions for TC genesis and intensification (Elsner et al. 2008; Knutson et al. 2019; Knutson et al. 2010; Kossin et al. 2013; Walsh et al. 2016).

The physical mechanisms underlying TC development can be framed in terms of interactions among radiation, surface fluxes, wind, and moist static energy (Wing et al. 2016). Local diabatic heating through reduced longwave cooling and enhanced surface fluxes typically promotes TC growth (Carstens and Wing 2020; Dai et al. 2025; Hsieh et al. 2023; Hsu and Wu 2025; Rios et al. 2025; Ruppert et al. 2020; Vecchi et al. 2019; Wing 2022; Wing et al. 2016; Wu and Soden 2024; Wu et al. 2021; Zhang et al. 2023; Zhang et al. 2021). Beyond these local processes, the geographic distribution of TCs is sensitive to the spatial pattern of SST anomalies (Eusebi et al. 2025; Hsieh et al. 2024; Kieu et al. 2023; Vecchi and Soden 2007; Zhao and Knutson 2024). For instance, a persistent “La Niña-like” warming pattern may increase near-term TC hazards in coastal Asia and the Atlantic basin (Lin et al. 2025). However, global climate models often exhibit biases in SST spatial patterns compared to observations (Wills et al. 2022; Zhuo et al. 2025), and the origins of these biases remain unclear.

While SST spatial patterns shape TC distribution, the response to uniform SST warming provides an important baseline for understanding thermodynamic and dynamical controls on TCs. Advances in high-performance computing and modeling have enabled the development of high-resolution models (with grid spacing ~25 km or finer), which have led to overall improvements in the simulation of TCs (Chen and Lin 2013; Murakami et al. 2015; Roberts et al. 2020; Roberts et al. 2025a; Vecchi et al. 2019). While global cloud-resolving models explicitly resolve deep convection, their computational cost limits long-term experiments. As a practical alternative, high-resolution climate models have been proposed as a bridge between coarse-resolution simulations and cloud-resolving models (Roberts et al. 2025b). These models offer an opportunity to investigate TC responses to changes in the background climate state, and further exploration using state-of-the-art modeling frameworks is ongoing.

In this study, we use a 25-km resolution global TC-permitting model (AM2.5-25km) to investigate TC responses to uniform SST warming, with a focus on changes in TC intensity. We demonstrate that stronger TCs under warming arise not only from increases in potential intensity (PI)—the thermodynamic upper bound on storm strength—but also from increases in relative intensity (r), defined as the ratio of realized TC intensity to PI. This highlights the need to account for both thermodynamic limits and storm efficacy when assessing TC risks in a warming climate. Section 2 describes the model and methods. Section 3 show the results. We summarize our findings and add discussion in Section 4.

2. Methods

2.1 Model and Experiment

The AM2.5 model, developed at the NOAA's Geophysical Fluid Dynamics Laboratory, serves as the atmospheric component of the CM2.5 ocean-atmosphere coupled model (Delworth 2012; Putman and Lin 2007). In this study, we use a high-resolution version of AM2.5 with a horizontal grid spacing of approximately 25 km (referred to as AM2.5-25km), with output regridded to 0.3125° longitude by 0.25° latitude for analysis. When driven by historical SSTs, AM2.5-25km realistically captures the annual cycle (Yang et al. 2021), the geographic distribution (Hsieh et al. 2022), and past multidecadal variations in TCs (Chan et al. 2021; Kortum et al. 2024) compared to observations.

We begin with a Control simulation that uses prescribed monthly climatological SSTs and sea ice from the Hadley Centre Sea Ice and Sea Surface Temperature (HadISST) dataset (Rayner et al. 2003), averaged over the 20-year period from 1986 to 2005. To assess TC responses to warming, we conduct a second simulation (plus2K) in which a uniform 2 K increase is added to the climatological SSTs. Each simulation is integrated for 50 years. To assess changes in large-scale environmental conditions, we also analyze simulations from the Atmospheric Model Intercomparison Project (AMIP), a component of the CMIP6 baseline experiments (Eyring et al. 2016), along with corresponding simulations forced with a uniform 4 K increase in SSTs (amip-p4K). Additional details of these simulations are provided in Supplementary Table 1.

2.2 TC Tracker

TCs simulated in AM2.5-25km are tracked by a method developed by Harris et al. (2016). This method uses instantaneous 6-hourly outputs of sea level pressure, mid-tropospheric temperature, 850 hPa vorticity, and 10-m zonal and meridional winds to track high cyclonic vorticity features. Typically, the high cyclonic vorticity is accompanied with a sea-level pressure minimum, a warm core in the middle troposphere and strong near-surface winds. The threshold regarding 10-meter maximum wind speed is set as 17 m s^{-1}. In addition, we set the minimum warm core temperature anomaly relative to the surrounding environment at 2K. The parameters settings are consistent with Vecchi et al. (2019) to capture a global TC frequency consistent with observations in this model. AM2.5-25km can simulate major TCs (Saffir-Simpson Category 3–5) with lifetime maximum intensity exceeding 50 m s^{-1}. In this study, we focus on the response of Category 3–5 storms to background warming.

2.3 PI and vPI Calculation

PI represents the theoretical maximum wind speed a TC can achieve, conceptualized by treating the storm as a thermodynamic heat engine. Because of its strong correlation with observed TC intensities, PI is widely used to diagnose and project TC climatology and variability. In this study, PI is computed following the algorithm of Gilford (2021), based on the formulation of Bister and Emanuel (1998). The calculation requires four primary inputs: SST, mean sea level pressure, and vertical profiles of atmospheric temperature and water vapor. SST is prescribed as the surface boundary condition, and specific humidity is used in place of mixing ratio. All inputs are taken from monthly means. Key assumptions and parameter choices include: 1) the ratio of surface

exchange coefficients of enthalpy to momentum is set to the default value of 0.9; 2) dissipative heating is included; 3) air parcels are assumed to ascend pseudo-adiabatically; 4) the minimum outflow pressure level is capped at 50 hPa. If a parcel remains convectively unstable at this level, the TC outflow level is assumed to be at 50 hPa, and the calculation is terminated. The algorithm outputs PI as a scaled gradient wind speed, using a default surface reduction factor of 0.8. It also provides the corresponding minimum central pressure, outflow temperature, and outflow pressure level.

While PI sets the theoretical upper bound on TC intensity, other environmental and storm-scale factors can inhibit intensification. In particular, ventilation, the intrusion of dry air into the storm's core, can inhibit TC intensification. This effect is commonly quantified using the ventilation index (VI; (Tang and Emanuel 2012)):

$$\mathrm{VI} = \frac{\mathrm{V_s}\chi_\mathrm{m}}{\mathrm{PI}} \tag{1}$$

where $\mathrm{V_s}$ is the magnitude of the vertical wind shear between 850 hPa and 200 hPa, and χ_m is the entropy deficit at 600 hPa:

$$\chi_\mathrm{m} = \frac{s_m^* - s_{m,env}}{s_{SST}^* - s_b} \tag{2}$$

where $s_m^* - s_{m,env}$ is the difference between the saturation entropy (with relative humidity = 1) and the environmental entropy at 600 hPa, $s_{SST}^* - s_b$ the difference between the saturation entropy at SST and the entropy of the boundary layer air parcel (surface air temperature at 2m; or surface air temperature). Details of the entropy calculation can be found in Tang and Emanuel (2012). To incorporate the weakening effect of ventilation on PI, Chavas (2017) introduced the concept of ventilated potential intensity (vPI). The full derivation is presented in Chavas (2017). An analytic solution for vPI as a function of PI and VI was later provided by Komacek et al. (2020) and Garcia et al. (2024), and formalized in Chavas et al. (2025):

$$\mathrm{vPI} = \left(\mathrm{x} + \frac{1}{3\mathrm{x}}\right)\mathrm{PI} \tag{3}$$

$$\mathrm{x} = \frac{1}{\sqrt{3}}\left\{\sqrt{\left[\left(\frac{\mathrm{VI}}{\mathrm{VI_{max}}}\right)^2 - 1\right]} - \left(\frac{\mathrm{VI}}{\mathrm{VI_{max}}}\right)\right\}^{\frac{1}{3}} \tag{4}$$

where VI_{max} is the threshold ventilation index above which vPI is zero. Following Hoogewind et al. (2020) and Chavas et al. (2025), we adopt $VI_{max} = 0.145$. In this study, we use equations (3) and (4) to compute vPI, providing a more physically realistic estimate of the maximum TC intensity by explicitly incorporating ventilation effects.

3. Results

Figure 1 shows the track density of major TCs, i.e., Category 3-5 TCs with lifetime maximum intensity (w_{max}) exceeding $50\ m\ s^{-1}$ from the Control and plus2K simulations. In the Control simulation (Figure 1a), major TC activity is concentrated primarily over the Indo-Pacific warm pool, including the western North Pacific and the South Indian Ocean, with comparatively lower activity in the North Atlantic and other basins. Under uniform 2K SST warming, the spatial distribution of major TCs remains broadly similar, but the track density increases across most active regions (Figure 1b). The difference plot highlights a global increase in Category 3–5 TC occurrence, with particularly notable increases over the western Pacific, South Indian Ocean, and parts of the North Atlantic (Figure 1c). These results suggest that uniform SST warming enhances environmental conditions favorable for the development of major TCs.

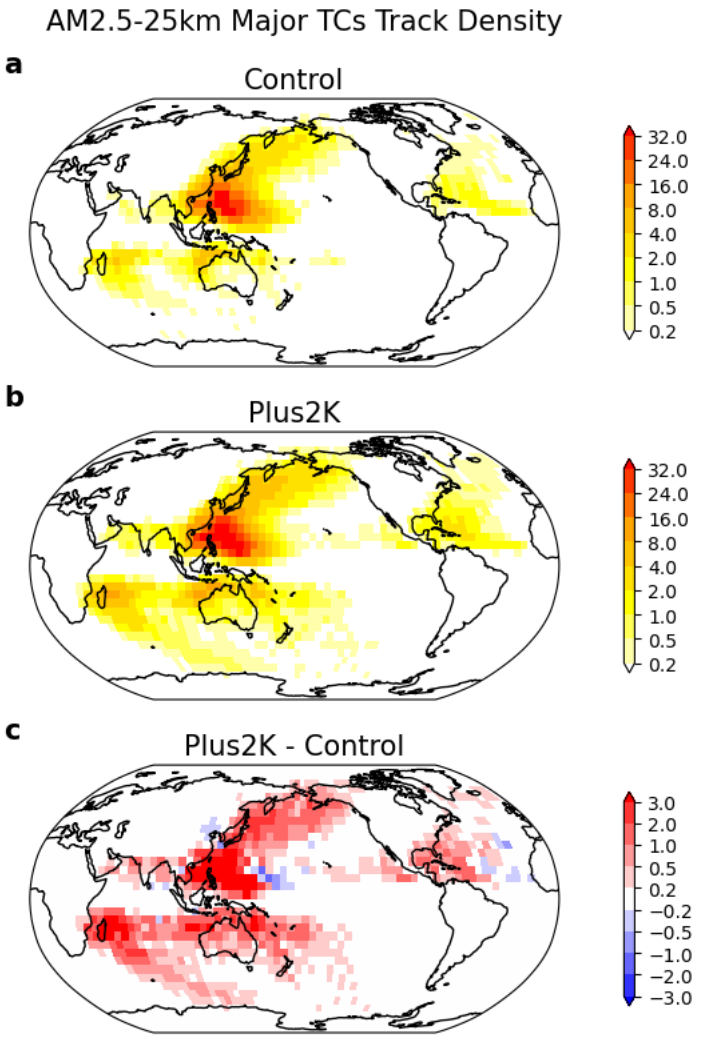

Figure 1 Maps of annual mean track density for major TCs (i.e., Category 3-5 TCs with $w_{max} \geq 50\ m\ s^{-1}$) in (a) Control, (b) plus2K, and (c) plus2K minus Control. Track density is computed as the number of Category 3–5 TC tracks within each $5° \times 5°$ boxes.

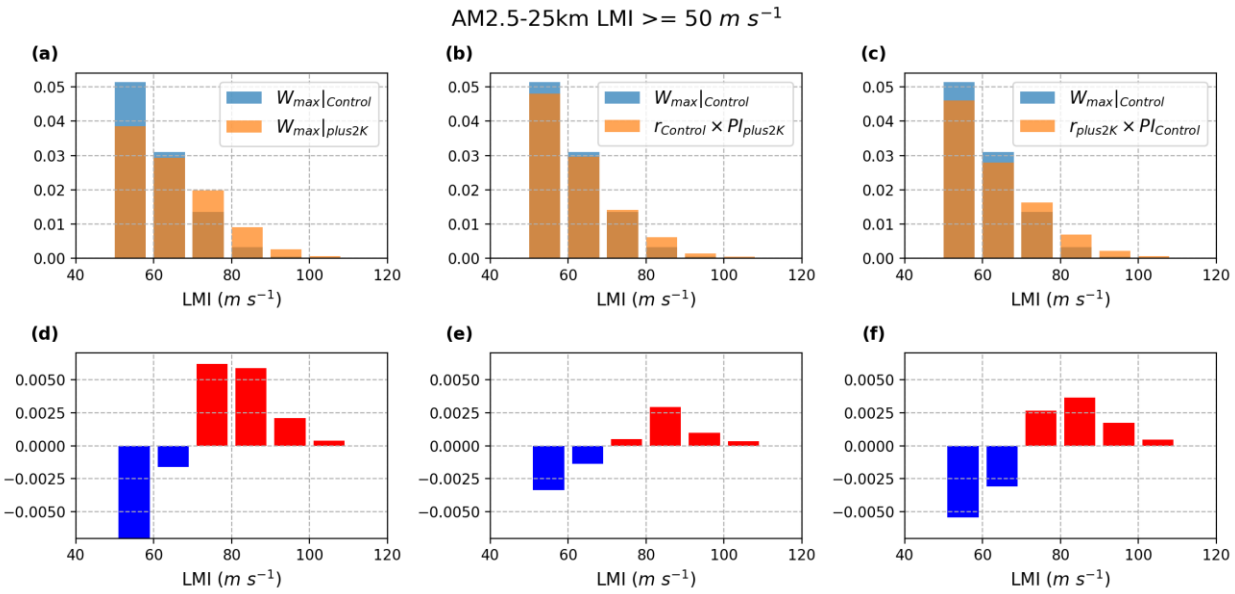

Figure 2 Lifetime maximum intensity probabilities distributions for (a) Control and plus2K, (b) Control and the reconstructed $w_{max}|_{p2K}$ computed by Eq. 4, and (c) Control and the reconstructed $w_{max}|_{p2K}$ computed by Eq. 5. The corresponding difference are shown in (d), (e) and (f) respectively.

We next examine changes in lifetime maximum intensity (w_{max}). With SST warming, the distribution of w_{max} shifts toward higher values, with instances of $w_{max}|_{plus2K}$ exceeding 70 m s^{-1} occurring more frequently (Figure 2a). To better interpret this shift, we analyze the role of relative intensity (r), defined as the ratio of a TC's w_{max} to its corresponding PI. The amplitude of r quantifies how efficiently a storm approaches its theoretical thermodynamic limit (DeMaria and Kaplan 1994). Given values of PI and r, the maximum wind speed of a TC can be calculated as:

$$w_{max} = r \times PI. \quad (5)$$

This relationship provides a framework for separating the contributions of PI and r to TC intensification under warming. For each simulation (Control and plus2K), Eq. 5 becomes $w_{max}|_{Control} = r_{Control} \times PI_{Control}$ and $w_{max}|_{plus2K} = r_{plus2K} \times PI_{plus2K}$.

To isolate the respective roles of PI and r in TC intensification, we reconstruct $w_{max}|_{plus2K}$ under two different assumptions:

1) Fixed r (using Control r) – isolating the effect of changes in PI, $w_{max}|_{plus2K\_fixed\_r} = r_{Control} \times PI_{plus2K}$;

2) Fixed PI (using Control PI) – isolating the effect of changes in r, $w_{max}|_{plus2K\_fixed\_PI} = r_{plus2K} \times PI_{Control}$.

This decomposition quantifies the relative contributions of thermodynamic potential (PI) and storm efficacy (r) to TC intensification in a warmer climate. Figure 2b compares $w_{max}|_{Control}$ and $w_{max}|_{plus2K\_fixed\_r}$, isolating the effect of increased PI while holding r constant. Under this scenario, the increase in TC intensity is attributed entirely to enhanced thermodynamic potential. The distribution of $w_{max}|_{plus2K\_fixed\_r}$ shifts clearly toward higher intensities (see Figure 2e for the difference), indicating that elevated PI alone can drive stronger storms under uniform SST warming. In contrast, Figure 2c compares $w_{max}|_{Control}$ and $w_{max}|_{plus2K\_fixed\_PI}$, isolating the impact of r by keeping PI fixed. This case represents a scenario where the large-scale environment remains unchanged, but TCs become more efficient at converting available energy into wind. The resulting distribution of $w_{max}|_{plus2K\_fixed\_PI}$ also shifts toward higher values (see Figure 2f for the difference), indicating that increased storm efficacy contributes to stronger TCs with SST warming. Together, these results demonstrate that both higher PI and enhanced r contribute substantially and complementarily to the increase in TC intensity under uniform SST warming.

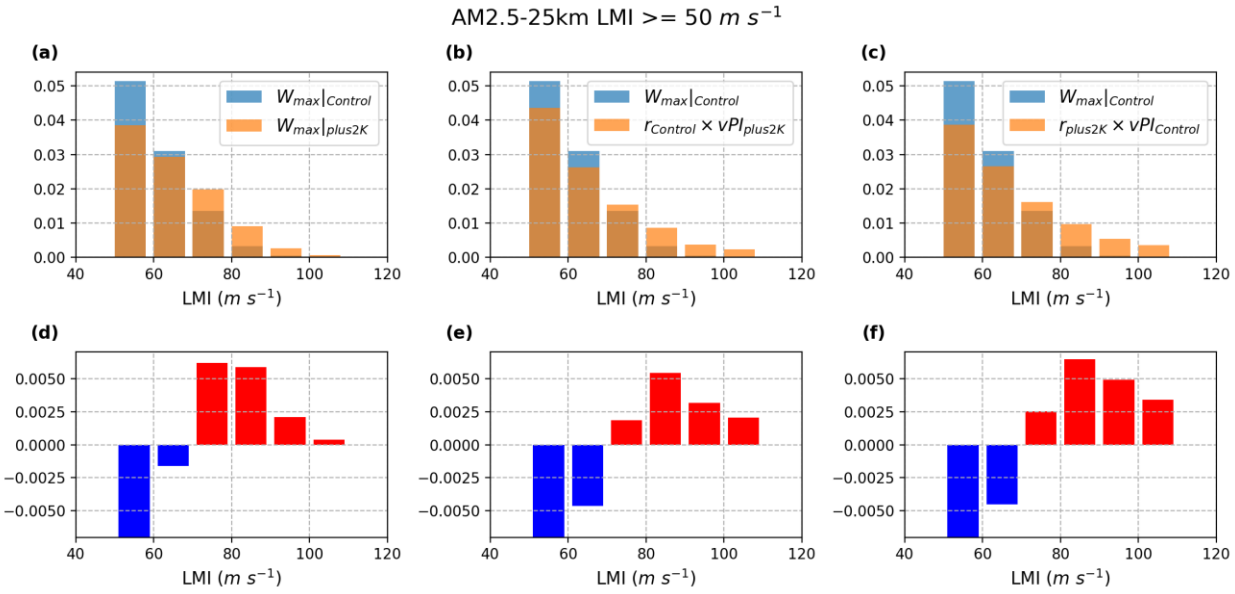

Figure 3 Same as Figure 2 but using vPI instead of PI.

To test whether ventilation alters this conclusion, we repeat the decomposition using vPI in place of PI (Figure 3). Results are qualitatively similar: both vPI and r changes contribute comparably to the shift of w_{max} towards larger values with SST warming (Figure 3e and 3f). This

consistency indicates that changes in TC efficacy under SST warming are largely insensitive to ventilation effects.

The combined contribution of higher PI and enhanced efficacy are also reflected in the rapid intensification process. Here, rapid intensification is measured by intensity change 24 hours before a TC's lifetime maximum intensity (w_{max}). We show that rapid intensification becomes stronger with SST warming, with 24-hour intensity change greater than 20 m s^{-1} happens more frequently in plus2K (Figure 4a). Similarly, to quantify the respective roles of PI and r in the rapid intensification process, we compute the intensity change in plus2K using $w_{max}|_{plus2K\_fixed\_r}$ in Figure 4b and $w_{max}|_{plus2K\_fixed\_PI}$ in Figure 4c. It shows that changes in PI are roughly twice as important as changes in efficacy in driving stronger rapid intensification in plus2K (Figure 4e and Figure 4f).

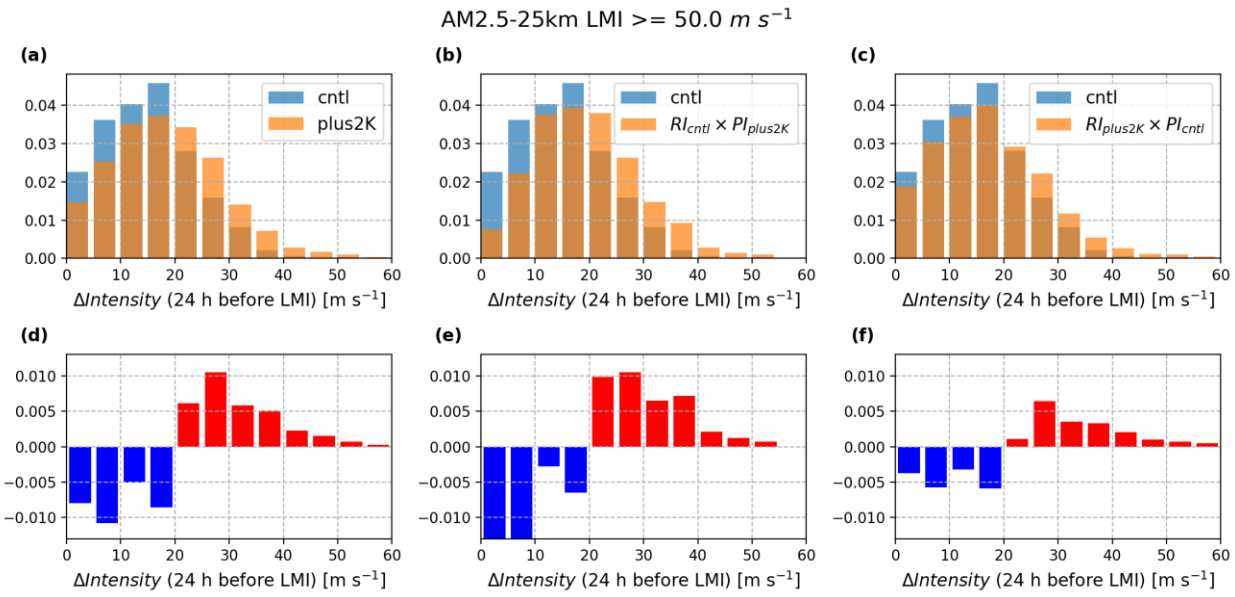

Figure 4 Intensity change 24 hours before LMI for (a) Control and plus2K, (b) Control and the reconstructed $w_{max}|_{p2K}$ computed by Eq. 4, and (c) Control and the reconstructed $w_{max}|_{p2K}$ computed by Eq. 5. The corresponding difference are shown in (d), (e) and (f) respectively.

So why does SST warming enhance the efficacy of TCs in gaining energy and drive stronger rapid intensification? One hypothesis is that warmer SST increases the probability of any given day having a major PI. In other words, the number of days with high PI values increase with SST warming. To test this, we calculate daily PI and count the number of days when PI exceeds a threshold indicative of conditions supportive of major TCs over a fixed seasonal window. For the

Northern Hemisphere, we consider June 1st to November 30th, and for the Southern Hemisphere it is January 1st to May 31st. Figure 5 shows that plus2K has substantially more high-PI days than Control, confirming that the probability of any given day having a major PI increases with SST warming. This increase is not unique to AM2.5-25km. To test the robustness of our results, we analyze daily PI from CMIP6 amip and amip-p4K experiments, which prescribe observed SSTs and uniformly warmed SSTs by +4 K, respectively. Nearly all models simulate an increase in high-PI days under +4 K SST warming (Figure 6), indicating that the thermodynamic availability of major TC conditions increases consistently across models. Together, the increased probability of major TCs can be attributed to increased probability of any given day having a major PI and increased probability of higher efficacy.

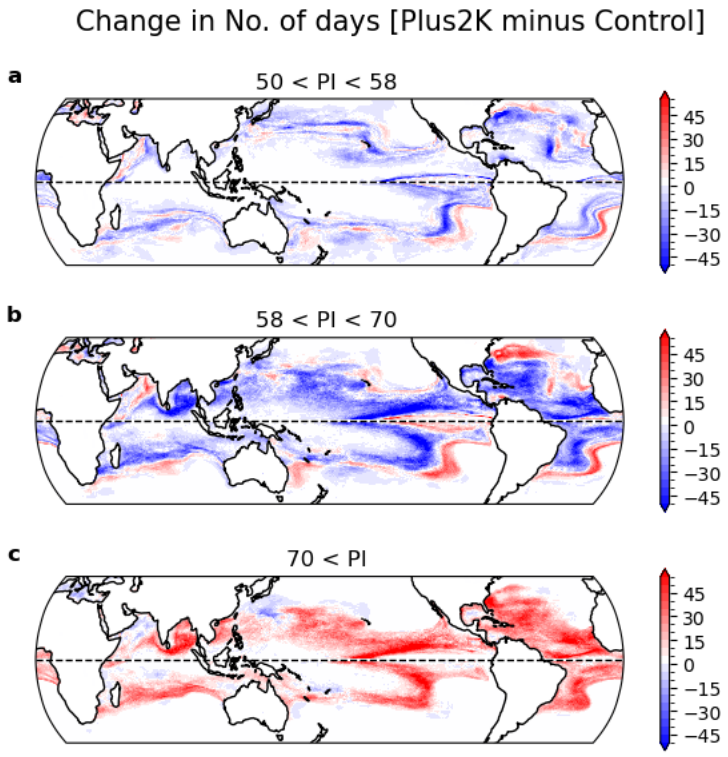

Figure 5 Change in number of days with (a) $50 < PI < 58\, m\, s^{-1}$, (b) $58 < PI < 70\, m\, s^{-1}$, and (c) $70 < PI$ between plus2K and Control in AM2.5-25km. Note the period of interest in the Northern Hemisphere is from June 1st to November 30th while that in the Southern Hemisphere is from January 1st to May 31st.

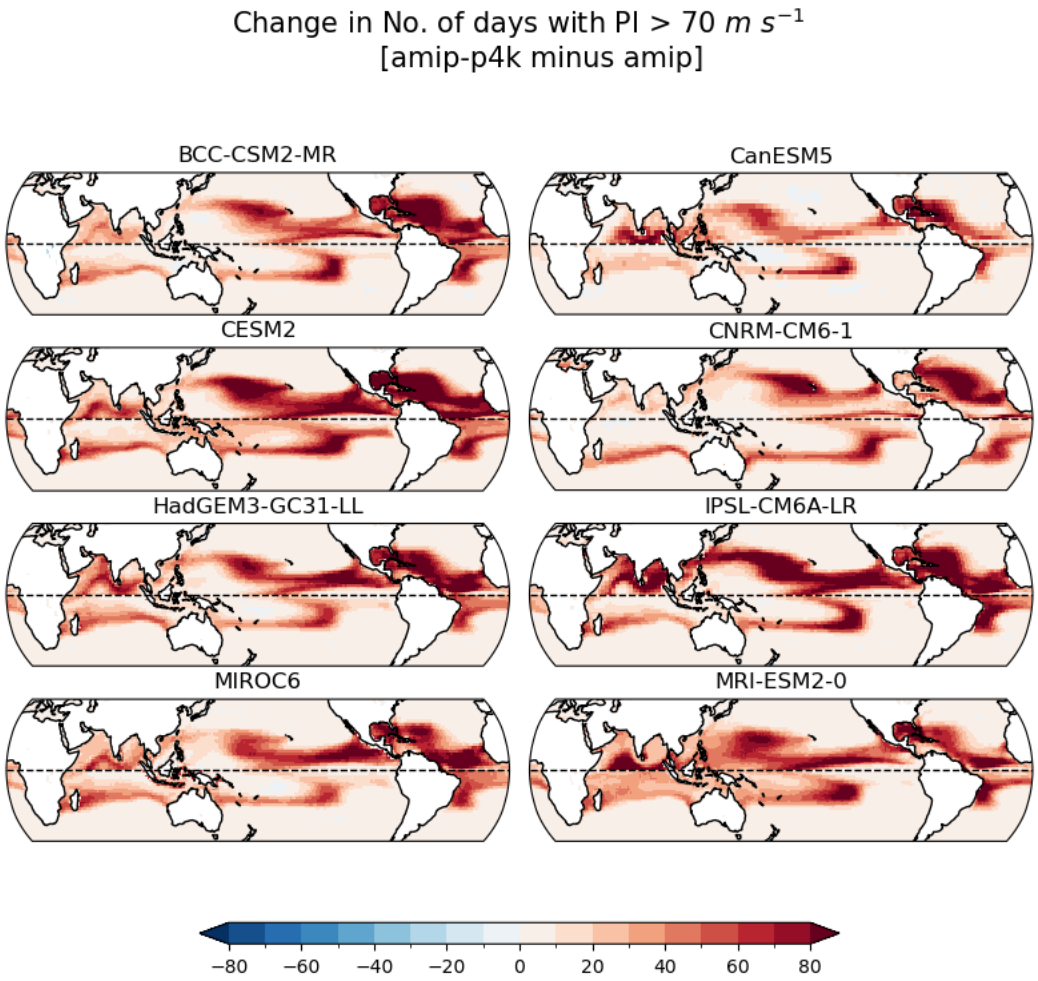

Figure 6 Change in the number of days with PI greater than $70\ m\ s^{-1}$ across the CMIP6 models.

4. Summary

We examine how major TCs, defined as Category 3–5 storms with lifetime maximum intensity (w_{max}) exceeding $50\ m\ s^{-1}$, respond to uniform SST warming using the high-resolution (25-km) global climate model AM2.5-25km. Under +2 K uniform SST warming, the frequency of major TCs increases notably, particularly over the western Pacific warm pool. In addition, the distribution of TC intensity shifts toward stronger storms, reflected by more cases reaching higher w_{max} values.

To diagnose the drivers of more intense TCs with SST warming, we focus on two metrics: potential intensity (PI), the thermodynamic upper bound on storm strength, and relative intensity (r) or efficacy, the ratio of actual intensity to PI. Decomposing changes in storm intensity reveals

that both enhanced PI and increased efficacy contribute substantially to TC strengthening. If PI rises while r remains fixed, intensification arises solely from higher thermodynamic potential. Conversely, if PI is fixed but r increases, intensification reflects improved efficacy in converting available energy into storm winds. Our analysis shows that while elevated PI strengthens storms, increased efficacy is also important. The rise in efficacy does not appear to result from mean changes in vertical wind shear or ventilation. Using ventilated PI (vPI), which accounts for the effect of dry-air intrusions, yields result consistent with the PI-based framework, confirming that the r increase is robust to large-scale circulation changes. The enhanced efficacy also contributes to stronger and more frequent rapid intensification events under SST warming.

In the plus2K simulation, the number of days when PI exceeds thresholds favorable for major TC development increases markedly. A similar increase in high-PI days is found across CMIP6 AMIP and AMIP-p4K simulations, underscoring the robustness of this response. Consequently, both the increased likelihood of higher efficacy and the increased frequency of high-PI conditions contribute to the greater probability of major TCs. This dual contribution suggests that assuming a simple proportionality between storm intensity and PI may underestimate future TC risks. Accurate projections of TC activity therefore require accounting for both rising thermodynamic limits and evolving storm–environment interactions, as captured by the efficacy with which TCs extract energy from their environment.

Acknowledgments

GAV and WY are supported in part by the Heising-Simons Foundation.

Availability Statement

The simulations were performed and archived on Princeton University's high-performance computing system. All data, including the tracked tropical cyclone outputs, are available upon request. The AM2.5-25km model code is publicly accessible at: https://www.gfdl.noaa.gov/cm2-5-and-flor-quickstart/.

References

Bhatia, K., and Coauthors, 2022: A potential explanation for the global increase in tropical cyclone rapid intensification. *Nature communications*, **13,** 6626.

Bister, M., and K. A. Emanuel, 1998: Dissipative heating and hurricane intensity. *Meteorology and Atmospheric Physics*, **65,** 233-240.

Camargo, S. J., M. K. Tippett, A. H. Sobel, C.-Y. Lee, B. Fosu, and K. I. Hodges, 2025: Tropical Cyclones and Associated Environmental Fields in CMIP6 models. *Journal of Climate*.

Camargo, S. J., and Coauthors, 2023: An update on the influence of natural climate variability and anthropogenic climate change on tropical cyclones. *Tropical Cyclone Research and Review*, **12,** 216-239.

Carstens, J. D., and A. A. Wing, 2020: Tropical cyclogenesis from self-aggregated convection in numerical simulations of rotating radiative-convective equilibrium. *Journal of Advances in Modeling Earth Systems*, **12,** e2019MS002020.

Chan, D., G. A. Vecchi, W. Yang, and P. Huybers, 2021: Improved simulation of 19th-and 20th-century North Atlantic hurricane frequency after correcting historical sea surface temperatures. *Science advances*, **7,** eabg6931.

Chavas, D. R., 2017: A simple derivation of tropical cyclone ventilation theory and its application to capped surface entropy fluxes. *Journal of the Atmospheric Sciences*, **74,** 2989-2996.

Chavas, D. R., S. J. Camargo, and M. K. Tippett, 2025: Tropical cyclone genesis potential using a ventilated potential intensity. *Journal of Climate*, **38,** 1667-1689.

Chen, J.-H., and S.-J. Lin, 2013: Seasonal predictions of tropical cyclones using a 25-km-resolution general circulation model. *Journal of Climate*, **26,** 380-398.

Dai, Y., D. S. Nolan, M. S. Torn, I. N. Williams, and W. D. Collins, 2025: Sensitivity of tropical cyclone intensity projections to longwave radiation. *Climate Dynamics*, **63,** 239.

Delworth, T. L., 2012: Simulated climate and climate change in the GFDL CM2.5 high-resolution coupled climate model. *J. Climate*, **25,** 2755-2781.

DeMaria, M., and J. Kaplan, 1994: Sea surface temperature and the maximum intensity of Atlantic tropical cyclones. *Journal of climate***,** 1324-1334.

Elsner, J. B., J. P. Kossin, and T. H. Jagger, 2008: The increasing intensity of the strongest tropical cyclones. *Nature*, **455,** 92-95.

Emanuel, K., 2021: Response of global tropical cyclone activity to increasing CO 2: Results from downscaling CMIP6 models. *Journal of Climate*, **34,** 57-70.

Emanuel, K. A., 1999: Thermodynamic control of hurricane intensity. *Nature*, **401,** 665-669.

Eusebi, R., G. A. Vecchi, W. Yang, and S. Fueglistaler, 2025: The Influence of Patterned Warming and CO 2 on North Atlantic Hurricane Frequency. *Journal of Climate*, **38,** 5391-5410.

Eyring, V., S. Bony, G. A. Meehl, C. A. Senior, B. Stevens, R. J. Stouffer, and K. E. Taylor, 2016: Overview of the Coupled Model Intercomparison Project Phase 6 (CMIP6) experimental design and organization. *Geoscientific Model Development*, **9,** 1937-1958.

Garcia, V., C. M. Smith, D. R. Chavas, and T. D. Komacek, 2024: Tropical cyclones on tidally locked rocky planets: Dependence on rotation period. *The Astrophysical Journal*, **965,** 5.

Gilford, D. M., 2021: pyPI (v1.3): Tropical Cyclone Potential Intensity Calculations in Python. *Geosci. Model Dev.*, **14,** 2351-2369.

Harris, L. M., S.-J. Lin, and C. Tu, 2016: High-resolution climate simulations using GFDL HiRAM with a stretched global grid. *Journal of Climate*, **29,** 4293-4314.

Hoogewind, K. A., D. R. Chavas, B. A. Schenkel, and M. E. O'Neill, 2020: Exploring controls on tropical cyclone count through the geography of environmental favorability. *Journal of Climate*, **33,** 1725-1745.

Hsieh, T.-L., W. Yang, G. A. Vecchi, and M. Zhao, 2022: Model spread in the tropical cyclone frequency and seed propensity index across global warming and ENSO-like perturbations. *Geophys. Res. Lett.*, **49,** e2021GL097157.

Hsieh, T.-L., G. A. Vecchi, C. Wang, W. Yang, B. Zhang, and B. J. Soden, 2024: Dependence of tropical cyclone seeds and climate sensitivity on tropical cloud response. *Science Advances*, **10,** eadi2779.

Hsieh, T.-L., B. Zhang, W. Yang, G. A. Vecchi, M. Zhao, B. J. Soden, and C. Wang, 2023: The Influence of Large-Scale Radiation Anomalies on Tropical Cyclone Frequency. *Journal of climate***,** 1-24.

Hsu, C.-K., and C.-C. Wu, 2025: Exploring the Role of Cloud Radiative Feedback in Tropical Cyclogenesis Utilizing Satellite and Reanalysis Datasets. *Journal of the Atmospheric Sciences*, **82,** 1137-1160.

Kieu, C., M. Zhao, Z. Tan, B. Zhang, and T. Knutson, 2023: On the role of sea surface temperature in the clustering of global tropical cyclone formation. *Journal of Climate*, **36,** 3145-3162.

Knutson, T., and Coauthors, 2019: Tropical cyclones and climate change assessment: Part I: Detection and attribution. *Bulletin of the American Meteorological Society*, **100,** 1987-2007.

——, 2020: Tropical cyclones and climate change assessment: Part II: Projected response to anthropogenic warming. *Bulletin of the American Meteorological Society*, **101,** E303-E322.

Knutson, T. R., and Coauthors, 2010: Tropical cyclones and climate change. *Nature geoscience*, **3,** 157.

Komacek, T. D., D. R. Chavas, and D. S. Abbot, 2020: Hurricane genesis is favorable on terrestrial exoplanets orbiting late-type M dwarf stars. *The Astrophysical Journal*, **898,** 115.

Kortum, G., G. A. Vecchi, T.-L. Hsieh, and W. Yang, 2024: Influence of weather and climate on multidecadal trends in Atlantic hurricane genesis and tracks. *Journal of Climate*, **37,** 1501-1522.

Kossin, J. P., T. L. Olander, and K. R. Knapp, 2013: Trend analysis with a new global record of tropical cyclone intensity. *Journal of Climate*, **26,** 9960-9976.

Lin, J., C.-Y. Lee, S. J. Camargo, A. H. Sobel, and J.-Y. Zhuo, 2025: The response of tropical cyclone hazard to natural and forced patterns of warming. *npj Climate and Atmospheric Science*, **8,** 109.

Murakami, H., and Coauthors, 2015: Simulation and prediction of category 4 and 5 hurricanes in the high-resolution GFDL HiFLOR coupled climate model. *Journal of Climate*, **28,** 9058-9079.

Putman, W. M., and S.-J. Lin, 2007: Finite-volume transport on various cubed-sphere grids. *Journal of Computational Physics*, **227,** 55-78.

Rayner, N., and Coauthors, 2003: Global analyses of sea surface temperature, sea ice, and night marine air temperature since the late nineteenth century. *Journal of Geophysical Research: Atmospheres*, **108**.

Rios, G., G. Vecchi, and W. Yang, 2025: Reducing tropical cyclone activity in global climate models by evaporative suppression. *Journal of Geophysical Research: Atmospheres*, **130,** e2024JD043302.

Roberts, M. J., and Coauthors, 2020: Projected future changes in tropical cyclones using the CMIP6 HighResMIP multimodel ensemble. *Geophysical research letters*, **47,** e2020GL088662.

Roberts, M. J., and Coauthors, 2025a: High-Resolution Model Intercomparison Project phase 2 (HighResMIP2) towards CMIP7. *Geoscientific Model Development*, **18,** 1307-1332.

Roberts, M. J., and Coauthors, 2025b: High-Resolution Model Intercomparison Project phase 2 (HighResMIP2) towards CMIP7. *Geosci. Model Dev.*, **18,** 1307-1332.

Ruppert, J. H., A. A. Wing, X. Tang, and E. L. Duran, 2020: The critical role of cloud–infrared radiation feedback in tropical cyclone development. *Proceedings of the National Academy of Sciences*, **117,** 27884-27892.

Song, J., Y. Duan, and P. J. Klotzbach, 2020: Increasing trend in rapid intensification magnitude of tropical cyclones over the western North Pacific. *Environmental Research Letters*, **15,** 084043.

Tang, B., and K. Emanuel, 2012: A ventilation index for tropical cyclones. *Bulletin of the American Meteorological Society*, **93,** 1901-1912.

Vecchi, G. A., and B. J. Soden, 2007: Effect of remote sea surface temperature change on tropical cyclone potential intensity. *Nature*, **450,** 1066-1070.

Vecchi, G. A., and Coauthors, 2019: Tropical cyclone sensitivities to CO 2 doubling: roles of atmospheric resolution, synoptic variability and background climate changes. *Climate Dynamics*, **53,** 5999-6033.

Walsh, K. J., and Coauthors, 2016: Tropical cyclones and climate change. *Wiley Interdisciplinary Reviews: Climate Change*, **7,** 65-89.

Wills, R. C., Y. Dong, C. Proistosecu, K. C. Armour, and D. S. Battisti, 2022: Systematic climate model biases in the large-scale patterns of recent sea-surface temperature and sea-level pressure change. *Geophysical Research Letters*, **49,** e2022GL100011.

Wing, A. A., 2022: Acceleration of tropical cyclone development by cloud-radiative feedbacks. *Journal of the Atmospheric Sciences*, **79,** 2117-2137.

Wing, A. A., S. J. Camargo, and A. H. Sobel, 2016: Role of radiative–convective feedbacks in spontaneous tropical cyclogenesis in idealized numerical simulations. *Journal of the Atmospheric Sciences*, **73,** 2633-2642.

Wu, S. N., and B. J. Soden, 2024: Radiative feedback from dry environmental air accelerates tropical cyclogenesis. *Geophysical Research Letters*, **51,** e2024GL110143.

Wu, S. N., B. Soden, and D. Nolan, 2021: Examining the Role of Cloud Radiative Interactions in Tropical Cyclone Development Using Satellite Measurements and WRF Simulations. *Geophysical Research Letters*, **48,** e2021GL093259.

Yang, W., T.-L. Hsieh, and G. A. Vecchi, 2021: Hurricane annual cycle controlled by both seeds and genesis probability. *Proc. Natl. Acad. Sci. USA*, **118,** e2108397118.

Zhang, B., B. J. Soden, and G. A. Vecchi, 2023: A Vertically Resolved Analysis of Radiative Feedbacks on Moist Static Energy Variance in Tropical Cyclones. *Journal of Climate*, **36,** 1125-1141.

Zhang, B., B. J. Soden, G. A. Vecchi, and W. Yang, 2021: The role of radiative interactions in tropical cyclone development under realistic boundary conditions. *Journal of Climate*, **34,** 2079-2091.

Zhao, M., and T. Knutson, 2024: Crucial role of sea surface temperature warming patterns in near-term high-impact weather and climate projection. *npj Climate and Atmospheric Science*, **7,** 130.

Zhuo, J.-Y., and Coauthors, 2025: A more la Niña–like response to radiative forcing after flux adjustment in CESM2. *Journal of Climate*, **38,** 1037-1050.